CellPress

Cancer Cell
Article

A Functional Genomic Approach Identifies *FAL1* as an Oncogenic Long Noncoding RNA that Associates with BMI1 and Represses p21 Expression in Cancer

Xiaowen Hu,[1,2,3] Yi Feng,[4] Dongmei Zhang,[1,2,8] Sihai D. Zhao,[10] Zhongyi Hu,[1,2] Joel Greshock,[4] Youyou Zhang,[1,2] Lu Yang,[1,2,9] Xiaomin Zhong,[1,2,11] Li-Ping Wang,[5] Stephanie Jean,[3] Chunsheng Li,[1,2] Qihong Huang,[12] Dionyssios Katsaros,[13] Kathleen T. Montone,[5] Janos L. Tanyi,[3] Yiling Lu,[15] Jeff Boyd,[14] Katherine L. Nathanson,[6] Hongzhe Li,[7] Gordon B. Mills,[15] and Lin Zhang[1,2,3,*]

[1]Ovarian Cancer Research Center
[2]Center for Research on Reproduction & Women's Health
[3]Department of Obstetrics and Gynecology
[4]Abramson Family Cancer Research Institute
[5]Department of Pathology and Laboratory Medicine
[6]Department of Medicine
[7]Department of Biostatistics and Epidemiology
Perelman School of Medicine, University of Pennsylvania, Philadelphia, PA 19104, USA
[8]State Key Laboratory of Biotherapy
[9]Department of Obstetrics and Gynecology
West China Medical School, Sichuan University, Chengdu 610041, China
[10]Department of Statistics, University of Illinois at Urbana-Champaign, Champaign, IL 61820, USA
[11]Center for Stem Biology and Tissue Engineering, Department of Biology, Zhongshan School of Medicine, Sun Yat-sen University, Guangzhou 510080, China
[12]Wistar Institute, Philadelphia, PA 19104, USA
[13]Department of Obstetrics and Gynecology, University of Turin, Turin 10124, Italy
[14]Cancer Genome Institute, Fox Chase Cancer Center, Philadelphia, PA 19111, USA
[15]Department of Systems Biology, MD Anderson Cancer Center, Houston, TX 7705, USA
*Correspondence: linzhang@mail.med.upenn.edu
http://dx.doi.org/10.1016/j.ccr.2014.07.009

SUMMARY

In a genome-wide survey on somatic copy-number alterations (SCNAs) of long noncoding RNA (lncRNA) in 2,394 tumor specimens from 12 cancer types, we found that about 21.8% of lncRNA genes were located in regions with focal SCNAs. By integrating bioinformatics analyses of lncRNA SCNAs and expression with functional screening assays, we identified an oncogene, *f*ocally *a*mplified *l*ncRNA on chromosome *1* (*FAL1*), whose copy number and expression are correlated with outcomes in ovarian cancer. *FAL1* associates with the epigenetic repressor BMI1 and regulates its stability in order to modulate the transcription of a number of genes including *CDKN1A*. The oncogenic activity of *FAL1* is partially attributable to its repression of p21. *FAL1*-specific siRNAs significantly inhibit tumor growth in vivo.

INTRODUCTION

Cancer genomes are highly disorganized and harbor numerous somatic copy-number alterations (SCNAs) (Beroukhim et al., 2010; Zack et al., 2013). Although the majority of the copy number abnormalities are the consequence of genomic instability, a subset of SCNAs contributes to tumorigenesis. Systemic analyses using large-scale genomic profiles and genome-wide functional screening have been successfully applied to identifying cancer-driving SCNA loci that encode proteins (Beroukhim et al., 2010; Zack et al., 2013). However, protein-coding sequences occupy less than 2% of the human genome

Significance

Although up to 70% of the human genome is transcribed to RNA, only 2% carries protein-coding genes. In addition to miRNAs, recent studies of lncRNAs suggest that they may represent another important class of nonprotein regulators of tumorigenesis. However, research on the oncogenic roles of lncRNAs is limited. In the current study, we provide an in-depth description of lncRNA SCNAs in 12 types of cancer and describe an integrated approach of identifying lncRNA genes with oncogenic activity. Using this approach, we identified *FAL1* as an oncogenic lncRNA. Our studies have elucidated the molecular mechanism underlying the oncogenic activity of *FAL1* and provide proof-of-concept evidence for using *FAL1* as a cancer prognostic marker and therapeutic target.

(International Human Genome Sequencing Consortium, 2004), and many focal SCNAs in cancer have been mapped to "protein-coding gene desert" regions (Beroukhim et al., 2010; Zack et al., 2013).

Recent advances in high-throughput sequencing technology have revealed that the majority (~70%) of the human genome is transcribed to RNA, generating many thousands of noncoding transcripts (Derrien et al., 2012; Djebali et al., 2012). Long noncoding RNAs (lncRNAs) are operationally defined as RNA transcripts that are larger than 200 nt but do not appear to have protein-coding potential (Batista and Chang, 2013; Guttman and Rinn, 2012; Karreth and Pandolfi, 2013; Lee, 2012; Lieberman et al., 2013; Ørom and Shiekhattar, 2013; Prensner and Chinnaiyan, 2011; Ulitsky and Bartel, 2013). Similar to protein-coding transcripts, the transcription of lncRNAs is subject to typical histone-modification-mediated regulation, and lncRNA transcripts are processed by the canonical spliceosome machinery. Compared with their protein-coding counterparts, lncRNA genes are composed of fewer exons, under weaker selective constraints during evolution, and in relatively lower abundance. In addition, the expression of lncRNAs is strikingly cell type and tissue specific and, in many cases, even primate specific. To date, most of the well-characterized lncRNAs have been discovered serendipitously. The investigations on this small cohort of lncRNAs have demonstrated that these noncoding transcripts can serve as scaffolds or guides to regulate protein-protein or protein-DNA interactions (Engreitz et al., 2013; Gupta et al., 2010; Huarte et al., 2010; Jeon and Lee, 2011; Simon et al., 2013; Tsai et al., 2010; Yang et al., 2011, 2013b), as decoys to bind proteins (Di Ruscio et al., 2013; Hung et al., 2011; Tripathi et al., 2010, 2013) or microRNAs (miRNAs) (Hansen et al., 2013; Memczak et al., 2013; Poliseno et al., 2010; Tay et al., 2011), and as enhancers to influence gene transcription, when transcribed from the enhancer regions (enhancer RNA) (Kim et al., 2010; Li et al., 2013; Wang et al., 2011) or their neighboring loci (noncoding RNA activator) (Lai et al., 2013; Ørom et al., 2010). The biological processes affected by lncRNAs include cell proliferation (Hung et al., 2011; Tripathi et al., 2013), differentiation (Guttman et al., 2009; Guttman et al., 2011; Kretz et al., 2013; Loewer et al., 2010; Ulitsky et al., 2011), migration (Gupta et al., 2010; Ling et al., 2013; Ørom et al., 2010; Yang et al., 2013a), immune response (Carpenter et al., 2013; Gomez et al., 2013), and apoptosis (Huarte et al., 2010), all of which have been implicated in tumorigenesis. In addition to being higher deregulated in tumors (Du et al., 2013; Gupta et al., 2010; Prensner et al., 2011), lncRNAs have been found to act as tumor suppressors or oncogenes (Gupta et al., 2010; Ji et al., 2003; Ling et al., 2013; Pasmant et al., 2007; Prensner et al., 2011, 2013; Yang et al., 2013b; Yildirim et al., 2013). To characterize the landscape of lncRNA gene SCNAs across cancers, we repurposed the SNP microarray results from a total of 2,394 tumor specimens taken from 12 cancer types (Beroukhim et al., 2010) and analyzed the SCNAs of 13,870 lncRNA gene loci.

RESULTS

lncRNAs Exhibit Frequent SCNAs in Human Cancer

We analyzed the SNP arrays of a total of 2,394 tumor specimens from 12 cancer types in the Tumorscape database created by the Broad Institute (Beroukhim et al., 2010) (Table S1 and Figure S1A available online). The genomic locations of 13,870 lncRNAs (Table S2) were retrieved from an evidence-based lncRNA annotation provide by the GENCODE Consortium (Derrien et al., 2012), and the SCNA frequency of each lncRNA-containing locus was calculated. This revealed that the more frequently a lncRNA has a copy-number gain in a given tumor type, the less likely it would also have a high frequency of copy-number loss in the same tumor type (Figure S1B). As a result, when we define high-frequency gains or losses as alterations that take place in more than 25% of specimens from a given tumor type, few lncRNAs had both high-frequency gain and loss in the same type of tumor. Across the 12 tumor types, there were on average 12.0% and 7.6% of lncRNAs with high-frequency (i.e., in >25% of tumors) gain and loss, respectively (Figures 1A–1C; Table S3). Although small cell lung cancer had the largest number of high-frequency lncRNA SCNAs, myeloproliferative disorder had none (Figures 1B and 1C). Similar to the overall genomic alteration profiles, lncRNA SCNA profiles were cancer-type specific (Figure 1B; Figure S1A). Additionally, we analyzed the SNP arrays using a second lncRNA annotation generated by Cabili et al. (2011) (Table S2) and found the lncRNA SCNA frequency and tumor-type specificity were similar to that analyzed with GENCODE annotation (Figures S1C–S1E and Table S3). To further validate these findings, we acquired SNP arrays from The Cancer Genome Atlas (TCGA) project and analyzed lncRNA SCNAs in breast cancer. The lncRNA SCNA profiles in breast cancer samples from TCGA data sets were almost identical to those from the Broad Institute database (Figure S1F).

Two types of SCNAs are present in cancer genomes: those confined to a small genomic region are termed focal alterations, and those encompassing a large fragment, or even a whole chromosomal arm, are referred as broad (arm-level) alterations. Because focal alterations contain only a handful of genes and often exhibit high-amplitude variation, analyses of these alterations have led to the successful identification of cancer-causing genes (Beroukhim et al., 2010; Du et al., 2013). To screen for lncRNAs that may act as driver genes in tumorigenesis, we mapped lncRNA loci to 158 independent focal genomic alteration peaks (76 gains and 82 losses) that have been previously identified (Beroukhim et al., 2010). Totals of 1,064 and 1,953 lncRNAs were located in the regions with focal gains and losses, respectively (Tables S4 and S5). Although 995 lncRNAs were located in focal SCNA regions where cancer-associated protein-coding genes reside, we identified 2,022 (14.6%) lncRNAs in focal alteration regions that contain no known cancer-associated protein-coding genes (Tables S4 and S5). Importantly, within the top 20 most significant focal alteration peaks (Beroukhim et al., 2010), we identified 56 lncRNAs in focal gain regions and 132 lncRNAs in focal loss regions (Figure 1D). We reasoned that the lncRNAs that demonstrate high-frequency genomic alterations and/or reside in focal alteration loci are candidates for cancer-causing lncRNAs.

lncRNAs Are Widely Expressed in Human Cancer Cells

Because lncRNAs exert their functions as RNAs, we reasoned that the presence of RNA transcripts in cells should be a

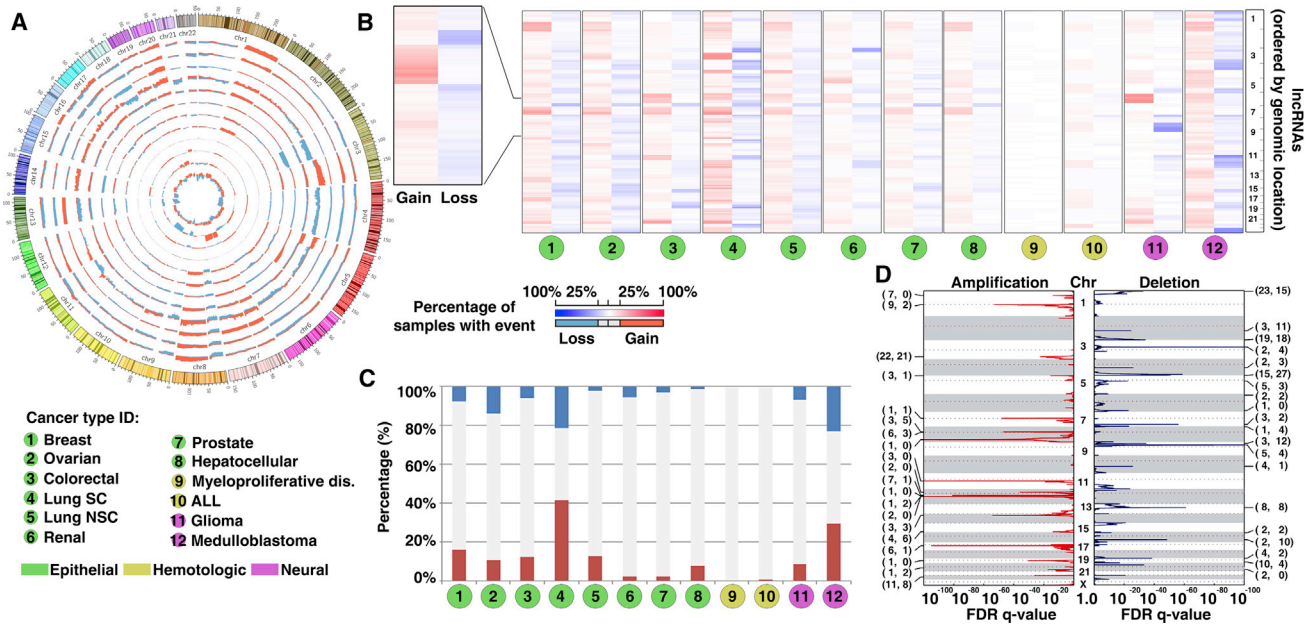

Figure 1. SCNAs of lncRNA in Cancers

(A) A genome-wide view of SCNAs in lncRNA-containing loci in cancers. Each track shows the frequency of lncRNA SCNAs in one cancer type. Red indicates gain; blue indicates loss. The outer and inner tracks represent cancer types 1 and 12, respectively.

(B) Heatmap of SCNA frequencies of lncRNA genomic loci in cancers. Each row represents one lncRNA, ordered by genomic location. Left, frequency of gain (red); right, frequency of loss (blue).

(C) Percentages of lncRNAs with significant copy-number alteration (>25% of specimens) in cancers.

(D) The lncRNAs and protein-coding genes in the top 20 most significant focal gain (left) or loss (right) peaks across cancers. The numbers of protein-coding genes (left) and lncRNAs (right) in each peak are indicated in parentheses. The independent focal genomic alteration peaks and the numbers of protein-coding genes in each peak were previously identified by the Tumorscape Project (Beroukhim et al., 2010).

See also Figure S1 and Tables S1, S2, S3, S4, S5, S6, and S7.

prerequisite for a lncRNA to be functional and that alterations in the genomic loci harboring lncRNAs with no detectable RNA transcripts are likely to be passenger events. We profiled 40 established cancer cell lines (across five cancer types) from the NCI60 cell line panel (Table S6) using a custom 60-mer oligonucleotide microarray with a total of 14,262 probes for 2,965 lncRNAs (an average of 5 probes for each lncRNA; Table S7), which were initially identified using the GENCODE annotation (Ørom et al., 2010). Probes for 11,081 protein-coding genes were also included in our microarray as controls. Overall, 41.7% of the lncRNA and 82.9% of the protein-coding gene probes were detected in 10 (25%) or more of the 40 cell lines; 23.8% of the lncRNA and 4.9% of the protein-coding gene probes were not detected in any cell line (Figure S1G). Among all the lncRNAs studied, about 17.8% were expressed in all 40 cancer cell lines. To validate the RNA expression results from microarray, we measured the RNA expression of 6 well-known lncRNAs in these cancer cell lines by quantitative RT-PCR (qRT-PCR) and found that there were strong correlations between the RNA expression measured by microarray and by PCR (Figure S1H). These findings demonstrate that lncRNAs are indeed widely expressed in cancers. Together, the cancer-cell-specific RNA expression information and the lncRNAs SCNA in multiple types of tumors can help us narrow down the list of cancer-causing lncRNA candidates by eliminating lncRNAs that do not express in cancer cells.

Clinically Guided Genetic Screening Identified *FAL1* as a Potential Oncogenic lncRNA

Next, we used the information obtained from the above genomic and transcriptomic analyses to select oncogenic lncRNA candidates for functional validation. The three criteria for candidate selection were as follows: (1) the lncRNA copy-number gain is observed in more than 25% of the samples in at least one type of tumors, (2) the lncRNA is located in a focal amplicon, and (3) the RNA expression of the candidate lncRNA is detected in more than 50% of cancer cell lines. The functional readout for the initial screening was in vitro clonogenicity. We hypothesized that short hairpin RNAs (shRNAs) targeting true oncogenic lncRNAs should greatly reduce the clonogenicity of cells, and shRNAs targeting bystander lncRNAs will have no effect. To minimize the possibility of observing off-target effects, we designed two independent shRNAs for each lncRNA candidate. In the initial clonogenic screening (Figure 2A), 37 lncRNA candidates were screened, and we found that both shRNAs targeting *ENSG00000228126* (focally amplified lncRNA on chromosome 1 [*FAL1*]), a lncRNA in a focal amplicon on chromosome 1q21.2 (Figures S2A and S2B), significantly reduced the clonogenicity of A2780 cells in a dose-dependent manner. Compared with *FAL1* shRNA1, shRNA2 was more efficient in knocking down endogenous *FAL1* expression (Figure 2B) and had a greater effect on inhibiting cell growth and colony formation (Figures 2A and 2B). Similar results were also observed in MDA-MB-231

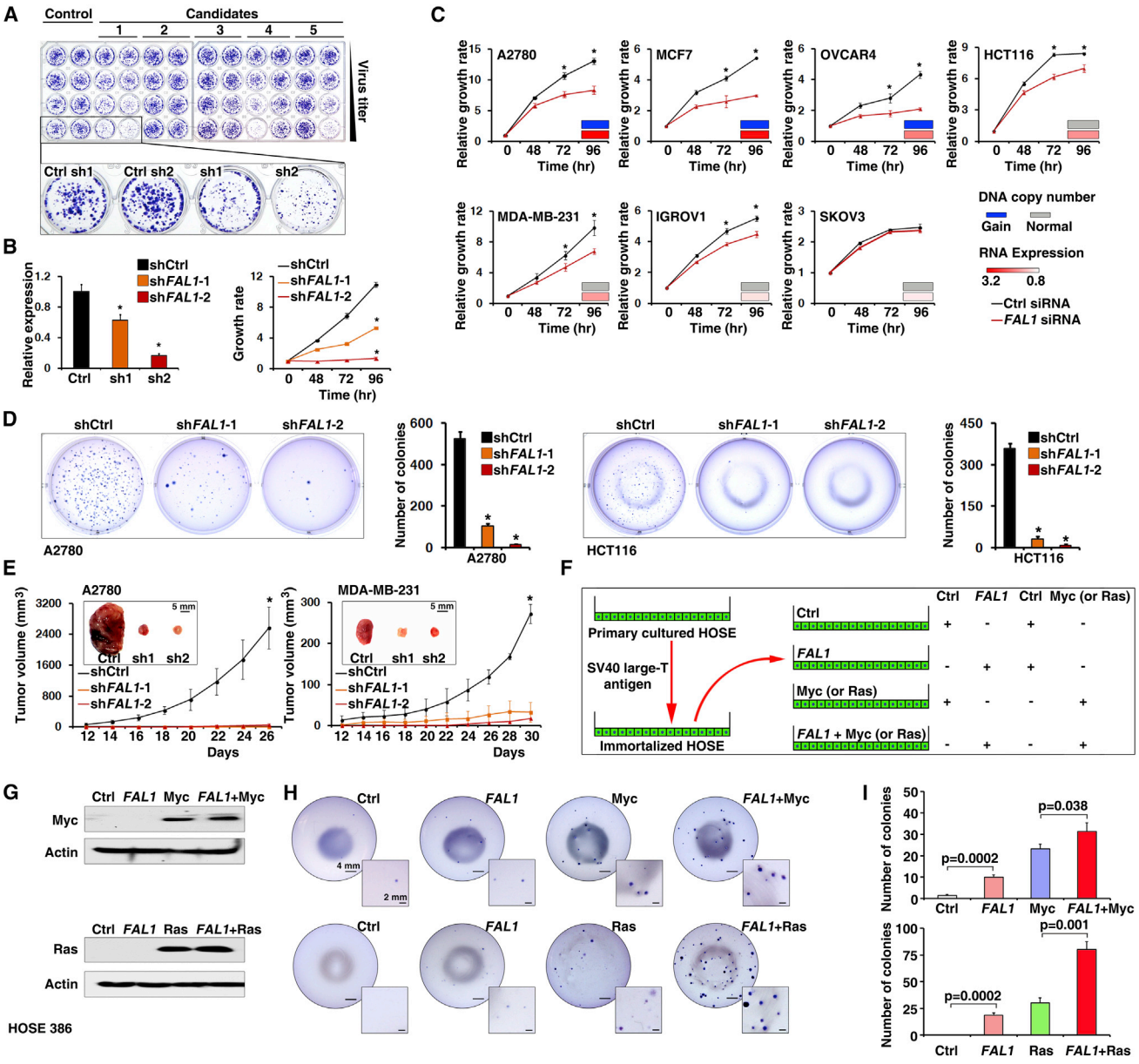

Figure 2. Identification and Validation of *FAL1* as a Potential Oncogenic lncRNA

(A) Representative results from clonogenic shRNA screening for oncogenic lncRNAs in A2780 (in 24-well plates). (Bottom) Wells with colonies expressing controls and *FAL1* hairpins.

(B) Relative expression of *FAL1* (left) and growth curve (right) of A2780 cells expressing control and *FAL1* shRNAs.

(C) Growth curves of seven cancer cell lines transfected with control or *FAL1* siRNAs. The *FAL1* SCNA status of each cell line is indicated as a blue (gain) or gray (normal) rectangle, and the relative *FAL1* expression in parental cells is indicated by the intensities of the pink rectangles.

(D). Soft-agar assay with cells expressing control and *FAL1* shRNAs (in 6-well plates).

(E) In vivo xenograft tumor growth curves of A2780 and MDA-MB-231 cells expressing control and *FAL1* shRNAs.

(F) Schematic diagram of the experimental design of testing the oncogenic potential of *FAL1*.

(G) The expression of Myc or Ras in HOSE cells transduced with *FAL1* alone or in combination with Myc or Ras.

(H and I) The representative result of soft-agar assay (H) and the corresponding quantification (I) on control cells and cells expressing *FAL1* alone or in combination with Myc or Ras.

Error bars indicate SD. *p < 0.05. See also Figure S2.

and HCT116 cells. Next, we validated the oncogenicity of *FAL1* in seven more cell lines that have a wide range of *FAL1* expression and various status of *FAL1* SCNA. With the exception of SKOV3 cells, which have normal copy number and low RNA expression of *FAL1*, all other cell lines were more or less dependent on the expression of *FAL1* for their growth (Figure 2C). Soft-agar assays further demonstrated that the expression of *FAL1* shRNAs significantly inhibited the anchorage-independent

growth of cancer cells (Figure 2D). Next, we demonstrated that the expression of *FAL1* shRNAs significantly suppressed the growth of subcutaneous tumors formed by A2780 or MDA-MB-231 cells in nude mice (Figure 2E).

We examined if *FAL1* expression is sufficient to promote transformation. We forced the expression of full-length *FAL1* cDNA (Figures S2C and S2D) in two independent batches of primary human ovarian surface epithelial (HOSE) cells and further transduced these *FAL1*-modified cells with Myc or Ras and their corresponding controls (Figures 2F and 2G). The oncogenicity of *FAL1* alone or in combination with Myc or Ras was evaluated in soft-agar assays. Although control HOSE cells form no colony in soft agar, cells expressing *FAL1* were able to form some colonies, although compared with those formed with Myc or Ras cells, the *FAL1* colonies were smaller and in fewer numbers (Figures 2F and 2G). Intriguingly, HOSE cells expressing *FAL1* in combination with Myc (or Ras) formed significantly more colonies than their single-gene expressing counterparts (Figures 2H and 2I; Figure S2E–S2Q). In aggregate, by integrating genomic and transcriptomic analysis with functional screening, we have successfully identified *FAL1* as a potential oncogenic lncRNA.

Interestingly, *FAL1* amplicon also contains a known protein-coding oncogene, *MCL1* (Beroukhim et al., 2010). We compared the mRNA levels of *MCL1* and five other genes within the *FAL1* locus in control and *FAL1* shRNA expressing A2780 cells and found that knocking down *FAL1* did not affect the expression of any of these neighboring genes (Figure S2R). This finding suggests that *FAL1* does not control the transcription of its neighboring genes; as such, the function of *FAL1* is likely independent to regulation of *MCL1* expression. It has been documented that a cluster of oncogenic lncRNAs, including *PCAT-1*, *CCAT2*, and *CARLo-5*, coamplify with *MYC*; yet they promote tumor growth via Myc-independent mechanisms (Kim et al., 2014; Ling et al., 2013; Prensner et al., 2011).

Expression and SCNA of *FAL1* Are Associated with Clinical Outcomes in Patients with Ovarian Cancer

An in-depth investigation of the SNP arrays revealed that the frequency of *FAL1* copy-number gain was remarkably high (49.7%) in epithelial tumors but much lower in neural (<19%) and hematologic (<6%) tumors (Figure 3A). Importantly, *FAL1* gene resides at a significant focal amplicon ($Q < 0.25$) on chromosome 1q21.2 in epithelial cancers (Figures 3A and 3B). To confirm these observations, we measured the copy number of *FAL1* in 99 cancer cell lines using quantitative PCR and observed *FAL1* copy-number gain in 46% of the cell lines (Figure 3C; Table S8). We then extracted the *FAL1* RNA expression data from the aforementioned custom RNA array containing 40 cancer cell lines and found a significant and positive correlation between the genomic copy number and RNA expression of *FAL1* ($R = 0.472$, $p = 0.002$; Figure 3D). It is also worth noting that several cell lines without *FAL1* amplification express high-level *FAL1* RNA. This observation suggests that *FAL1* RNA overexpression may be a common phenomenon in cancer cells and that mechanisms other than genomic amplification are present to cause *FAL1* RNA overexpression in cancer (Figure 3D).

To evaluate the clinical significance of *FAL1* in cancer, we characterized its expression and cellular location by in situ hybridization (ISH) using a *FAL1*-specific probe in a cohort of ovarian cancer specimens ($n = 181$, including 53 early-stage cases and 128 late-stage cases; Table S9). A *FAL1*-positive signal was detected in more than 93% of the specimens. Although 31.6% of the samples exhibited a strong signal, 37.5% and 23.9% had intermediate and weak signals, respectively (Figure 3E). *FAL1*-positive samples also exhibited a nuclear-enriched staining pattern, with a weak signal in cytoplasm. Similar staining patterns were also observed in cancer cell lines. We also characterized subcellular localization of *FAL1* by cell fractionation followed by qRT-PCR and observed the majority of *FAL1* RNA in the nuclear (Figure S3). Next, we measured *FAL1* RNA expression and genomic copy number using qPCR in ovarian tumors and found that both the *FAL1* RNA expression and genomic copy number in late-stage tumors were significantly higher than those in early-stage tumors (Figures 3F and 3G). Consistent with the observation from cell lines, there was a strong and positive correlation between *FAL1* RNA expression and its genomic copy number in the ovarian tumor specimens ($R = 0.577$, $p < 0.001$; Figure 3H). After stratifying the 128 late-stage ovarian cancer patients with *FAL1* RNA expression (cutoff, median expression) or gene amplification status, we found that both higher expression of *FAL1* RNA and genomic gain of *FAL1* gene were significantly associated with decreased survival in patients ($p < 0.0001$ and $p = 0.03$, respectively; Figure 3I). Taken together, these clinical findings demonstrated that gene amplification and RNA overexpression of *FAL1* occur frequently in epithelial cancer and are both associated with tumor progression in ovarian cancer.

FAL1 Associates with BMI1 Protein and Regulates Its Stability

To explore the molecular mechanisms underlying the oncogenic activity of *FAL1*, we sought to use RNA pull-down assay to identify proteins associated with *FAL1*. Briefly, biotinylated full-length *FAL1* or antisense transcript (negative control) synthesized by in vitro transcription was incubated with the nuclear lysate from A2780 cells, and coprecipitating proteins were isolated with streptavidin-agarose beads (Figure 4A). The RNA-associating proteins were resolved on SDS-PAGE gel, and the bands specific to *FAL1* were identified. BMI1, a 37 kD core subunit of the polycomb repressive complex 1 (PRC1) (Schuettengruber et al., 2007), was initially identified as a protein that was present only in *FAL1*-associated samples. To validate the association between BMI1 and *FAL1*, we subjected the lncRNA-pull-down protein samples to western blot with BMI1 antibody. A strong signal was observed in proteins pulled down with *FAL1* RNA but not in samples bound with either antisense *FAL1* or an unrelated fragment of *HOTAIR* (Figure 4B). To further confirm the interaction between *FAL1* and BMI1, we performed an RNA-immunoprecipitation (RNA-IP) assay, in which the RNA-BMI1 complex was immunoprecipitated using a BMI1 antibody. The amount of *FAL1* RNA in the coprecipitate was then measured by qRT-PCR. Compared with the immunoglobulin G (IgG)-bound sample, the BMI1-antibody-bound complex had a significant increase in the amount of *FAL1* RNA (Figures 4C and 4D). As negative controls, we also quantified the levels of two unrelated lncRNAs, *ENST00000457448* and *HOTAIR*, in the complexes coprecipitated by IgG or the BMI1 antibody. No significant

A

Cancer Subset	Location of Peak (Chromosome 1)	Q-value	Frequency of Amplification Overall	Focal
all_cancers	148692565-149042404	3.13E-53	0.3676	0.1089
all_epithelial	148692565-149042404	3.74E-43	0.4969	0.147
Hepatocellular	145279761-156420150	0.108	0.7107	0.0744
Breast	148152207-148996417	0.000326	0.6461	0.1687
Lung NSC	148397150-149275476	8.86E-31	0.6398	0.206
Lung SC	148692565-149696107	0.00471	0.575	0.225
Ovarian	148205369-149819296	0.0167	0.3786	0.165
Prostate	-	0.71	0.25	0.0978
Glioma	-	1	0.1951	0.0244
Medulloblastoma	-	1	0.1875	0.0156
Colorectal	143657867-170995569	0.171	0.1304	0.0373
Renal	-	1	0.127	0.0159
Acute lymphoblastic leukemia	-	1	0.0588	0.0026
Myeloproliferative disorder	-	0.749	0.0279	0.0047

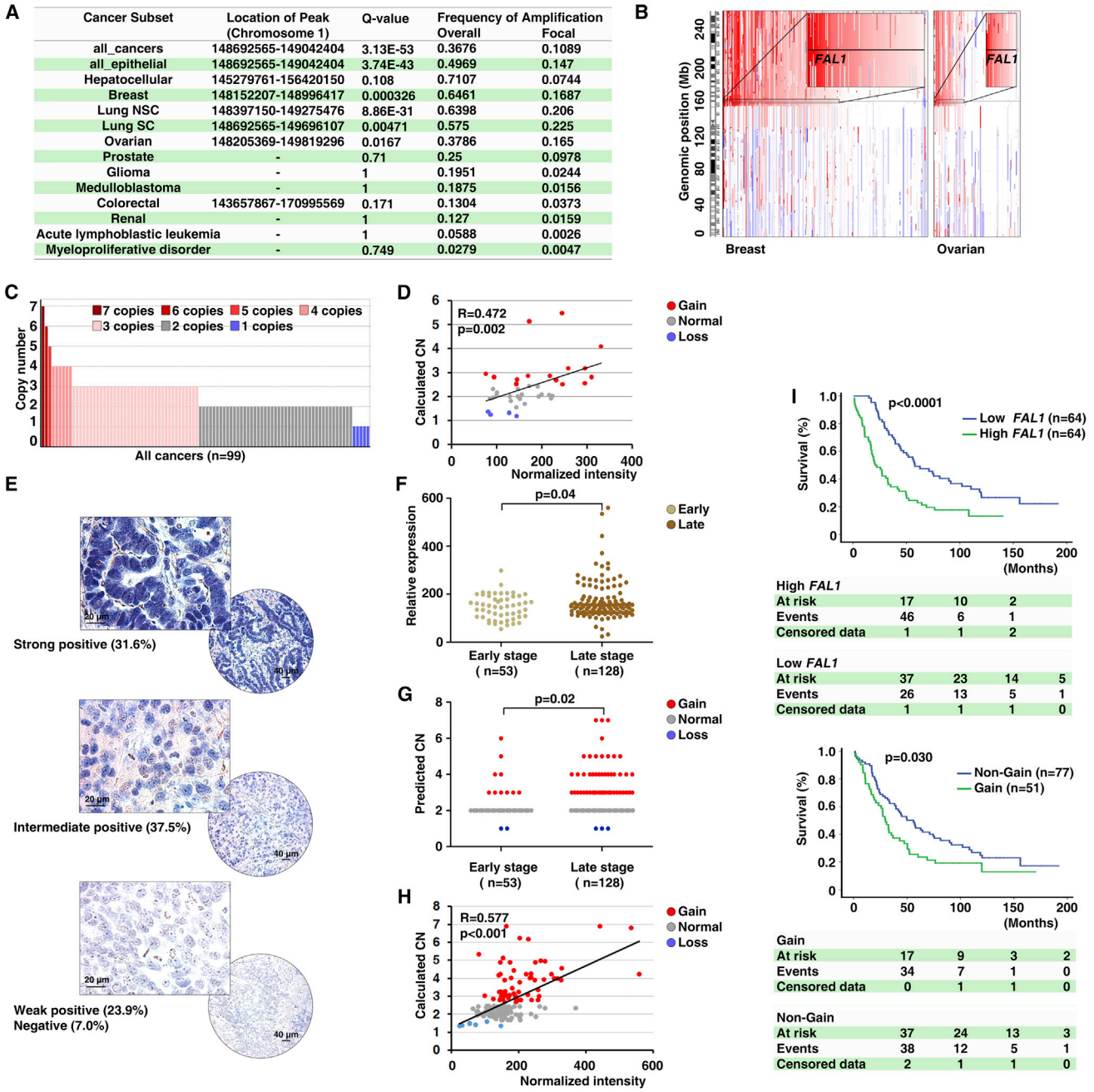

Figure 3. Characterization of *FAL1* Copy Number and RNA Expression in Cancers

(A) SCNAs of *FAL1* locus in cancers. Focal amplicons were identified by GISTIC analysis (Tumorscape).

(B) Copy-number profiles of chromosome 1q from breast and ovarian tumor specimens. Each sample is represented with a vertical line, and the positions of *FAL1* are noted with black horizontal lines. Red indicates gain; blue indicates loss.

(C) Copy numbers of *FAL1* in cancer cell lines (n = 99) were measured by qPCR.

(D) A correlation between *FAL1* gene copy number and RNA expression was observed in 40 cell lines.

(E) *FAL1* expression visualized by ISH in ovarian cancer.

(F) *FAL1* expression levels in early- and late-stage ovarian cancer specimens.

(G) Copy number of *FAL1* in the same cohort.

(H) A correlation between *FAL1* copy number and expression was observed in ovarian cancer specimens.

(I) Survival curves of late-stage ovarian cancer patients with high and low *FAL1* RNA expression (top) or different genomic SCNA status (bottom).

See also Figure S3 and Tables S8 and S9.

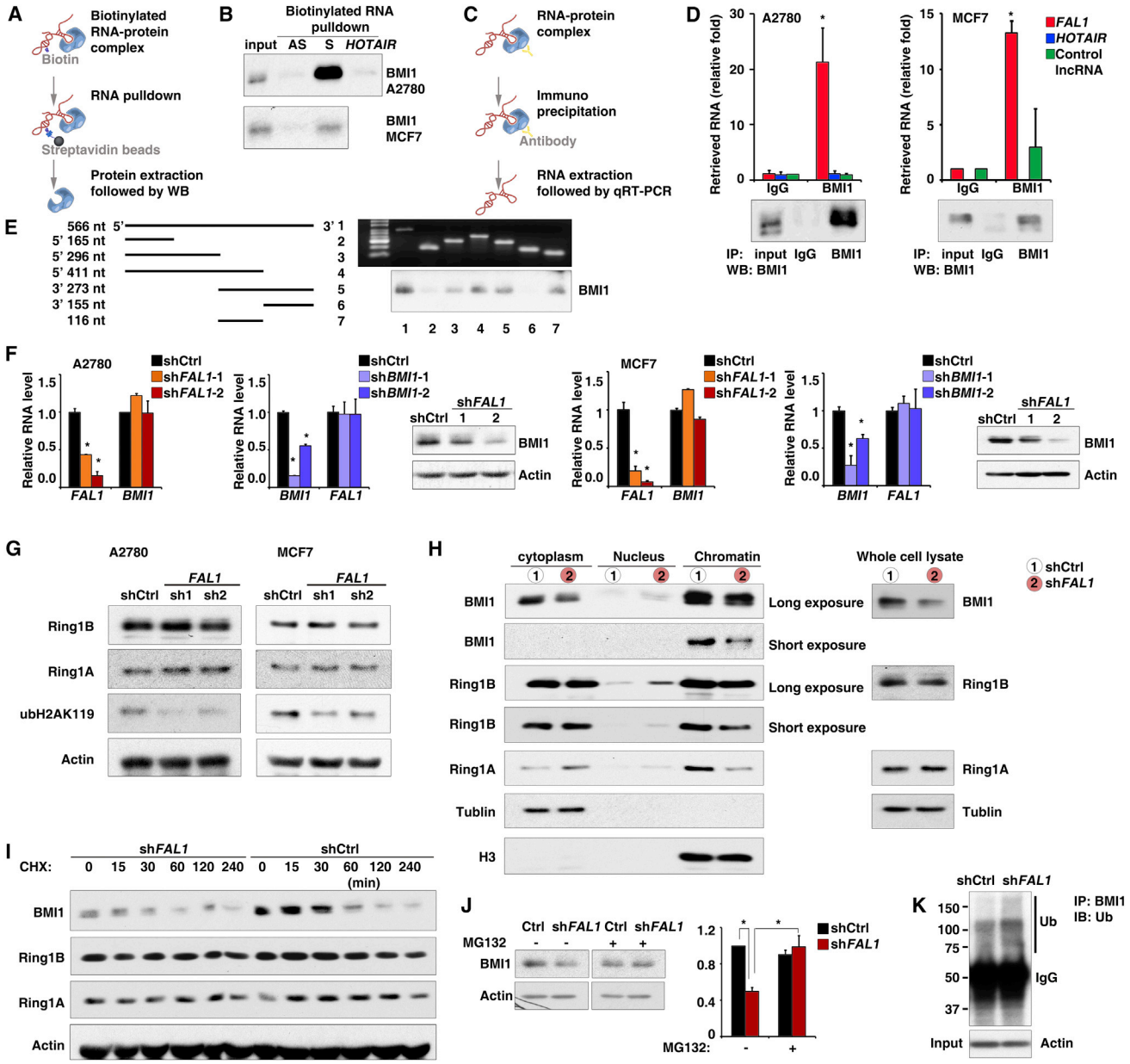

Figure 4. *FAL1* Associates with the BMI1 Protein and Regulates Its Stability

(A) A schematic representation of RNA pull-down.

(B) Western blot of BMI1 expression in 5% input and protein complexes pulled down by *FAL1*, antisense control, or unrelated control *HOTAIR* fragment from nuclear extracts.

(C) A schematic representation of an RNA immunoprecipitation assay.

(D) Results from RNA-IP and subsequent qRT-PCR assays. (Top) Relative quantification of *FAL1*, *HOTAIR*, and *ENST00000457448* in RNA-protein complexes immunoprecipitated with IgG or BMI1 antibodies from nuclear extracts. (Bottom) Representative western blot of BMI1 in the corresponding samples.

(E) Deletion mapping of BMI1-binding domain in *FAL1*. (Left) The schematic diagram of full-length and deleted fragments of *FAL1*; (right top) in vitro transcribed full-length and deleted fragments of *FAL1* showing correct sizes; (right bottom) western blot of BMI1 in protein samples pulled down by different *FAL1* fragments.

(F) Expression of *FAL1* and *BMI1* in A2780 (left) and MCF-7 (right) cells expressing shRNAs targeting these two genes.

(G) The expression of Ring1A, Ring1B, and ubiqintination of H2AK119 in A2780 (left) and MCF7 (right) cells expressing control and *FAL1* shRNAs.

(H) The levels of BMI1, Ring1A, and Ring1B in the cytoplasmic fraction, the soluble nuclear fraction, the chromatin-bound insoluble nuclear fraction of A2780 cells expressing control and *FAL1* shRNAs. Tubulin and H3 were used as cytoplasmic and chromatin-bound loading controls, respectively.

(I) The expression levels of BMI1, Ring1A, and Ring1B in control and *FAL1* knockdown cells treated with CHX.

(J) Western blot (left) and quantification (right) of BMI1 expression in control and *FAL1* knockdown cells treated with vehicle control or MG132.

(K) Western blot of BMI1-associated ubiquitination in control and *FAL1* knockdown cells treated with MG132.

Error bars indicate SD. *$p < 0.05$. See also Figure S4.

enrichment of either RNA was observed in the BMI1 complex (Figure 4D). Furthermore, using a series of deletion-mapping analyses, we identified a 116 nt region in the middle of the *FAL1* transcript (nt 296–411) as a major BMI1-binding domain, which is both required and sufficient for *FAL1*-BMI1 association (Figure 4E). Taken together, these results demonstrate that BMI1 is a *FAL1*-associated protein.

Next, we explored the molecular consequences of *FAL1*-BMI1 association. Although downregulation of *BMI1* mRNA expression via *BMI1* shRNAs had no effect on *FAL1* RNA levels, expressing *FAL1* shRNAs significantly reduced the protein level, but not the mRNA level, of BMI1 (Figure 4F). The level of two other PRC1 core proteins, Ring1A and Ring1B, were similar in control and *FAL1*-knockdown cells, and the level of ubH2AK119 was much lower in *FAL1*-knockdown cells than in control cells (Figure 4G). Although we detected a weak signal of Ring1B in the *FAL1*-protein complex from lncRNA pull-down assay, the signal of BMI1 in *FAL1*-protein complex was much stronger than that of Ring1B, and *FAL1*-mediated pull-down significantly enriched BMI1 but not Ring1B protein (Figure S4A). This observation suggests that the *FAL1*-BMI1 association may help specifically stabilize BMI1 protein. Additionally, we fractionated control and *FAL1*-knockdown cells and analyzed the protein levels of BMI1, Ring1A, and Ring1B in the cytoplasm, the soluble nuclear fraction, and the insoluble, chromatin-bound fraction. As shown in Figure 4H, there was a marked decrease of chromatic-bound BMI1, Ring1A, and Ring1B proteins in *FAL1*-knockdown cells than in controls. Concomitantly, there was a slight increase of these three PRC1 proteins in the soluble nuclear fraction in *FAL1*-knockdown cells than in control cells (Figure 4H). To further explore the mechanism of *FAL1*-mediated BMI1 regulation, we treated A2780 cells with cycloheximide (CHX) and analyzed the stabilities of BMI1, Ring1A and Ring1B in response to *FAL1* downregulation. Although the half-lives of Ring1A and Ring1B were not significantly affected by *FAL1* knockdown, the half-life of BMI1 was much shorter in *FAL1* knockdown cells than in controls (Figure 4I). The half-life of MDM2, a protein unrelated to PRC1 complex, was not affected by *FAL1* knockdown, suggesting that *FAL1* shRNA expressions does not affect protein half-lives globally (Figure S4B). In agreement with this observation, when MG132 was added into the culture medium to inhibit proteasome degradation, the endogenous BMI1 protein expression in *FAL1* knockdown cells was significantly increased and reached a level that was comparable to that in control cells (Figure 4J), and higher BMI ubiquitination levels were also observed in *FAL1* knockdown cells treated with MG132 (Figure 4K). In aggregate, these observations suggested that *FAL1* expression is important in regulating BMI1 protein stability.

FAL1 overexpression led to higher expression of BMI1 protein in HOSE cells (Figure S4C). Consistently, compared with control cells, *FAL1*-overexpressing cells had higher level of H2AK119 ubiquitination (Figure S4C). Further analysis on different subcellular fractions revealed that *FAL1*-expressing cells had higher BMI1 expression in all different fractions than control cells (Figure S4D). Interestingly, in response to *FAL1* overexpresion, there were also slight increases of Ring1A and Ring1B protein in the whole-cell lysates and in different subcellular fractions. However, the changes in Ring1A/B were to a much lesser extent than that in BMI1 (Figure S4C). Together, these findings suggest that the primary function of *FAL1* is to stabilize BMI1, and BMI1 stabilization, we reason, may further stabilize the whole PRC1 complex, therefore causing increases in the levels of other PRC1 core proteins.

FAL1 Regulates the Transcription of a Large Set of Genes

BMI1 is part of the PRC1 complex, a well-characterized chromatin-modifying complex that represses the transcription of a wide range of genes (Schuettengruber et al., 2007). Given that *FAL1* can bind to and stabilize BMI1 and that *FAL1* expression alteration changed the level of H2AK119 ubiquitination, we reasoned that *FAL1* expression alteration may influence BMI1 activity, which in turn can lead to genome-wide alterations in transcription. To test this hypothesis, we analyzed the RNA expression profiles of A2780 cells expressing shRNAs targeting either *FAL1* or *BMI1*. Two independent shRNA hairpins were used for each target gene to avoid off-target effects. The transcription of 732 genes (represented by 1,015 probes) was upregulated by the expression of both *BMI1* shRNAs in A2780 cells. In support of our hypothesis, we found that knocking down *FAL1* induced transcriptional alterations in a wide range of genes, including 887 genes (represented by 1,019 probes) whose expression was upregulated by both *FAL1* shRNAs (Figure 5A). Intriguingly, the expression of 641 of the 1,019 *FAL1*-induced probes (62.9%) was also increased by at least one of the *BMI1* shRNAs, with 285 (28%) probes induced by both *BMI1* shRNAs (Figure 5A). Only 59 (5.8%) probes were upregulated by *FAL1* knockdown but downregulated by the expression of at least one *BMI1* shRNA; within these 59 probes, only four (0.4%) were downregulated by both *BMI1* shRNAs (Figure 5A). The high degree of similarity between *FAL1*- and BMI1-mediated transcriptional repression strongly indicates a functional interaction between *FAL1* and BMI1, and the 285 probes whose expressions was upregulated by all four hairpins (Figure 5A) may be a common set of target genes shared by *FAL1* and BMI1.

To explore the functional processes that are affected by *FAL1*-mediated transcriptional regulation, we performed gene ontology (GO) analysis on the 887 genes that were upregulated by the knockdown of *FAL1*. The most significantly overrepresented biological processes included pathways involved in cell proliferation, death, and survival, as well as cellular movement and protein degradation (Figure 5B; Table S10). For example, genes involved in cell-cycle arrest and apoptosis, such as *CDKN1A*, *FAS*, *BTG2*, *TP53I3*, *FBXW7*, and *CYFIP2*, were found to be significantly upregulated by both *FAL1* and *BMI1* knockdown in the above array studies. The increased expression of these six target genes was further validated by qRT-PCR (Figures 5A and 5C). Given that the PRC1 complex regulates gene transcription by binding to promoter regions and modifying chromatin, we examined whether *FAL1* knockdown affected BMI1 occupancy of the promoter regions in these target genes. The effect of *FAL1* knockdown on the occupancy of BMI1 or ubiquitination levels of H2AK119 in the target gene promoters was evaluated using a chromatin immunoprecipitation (ChIP) assay followed by qPCR. Among the six target genes tested, BMI1 occupancy and ubiquitinated H2AK119 were validated in the promoter regions of five genes, and knocking down *FAL1* significantly

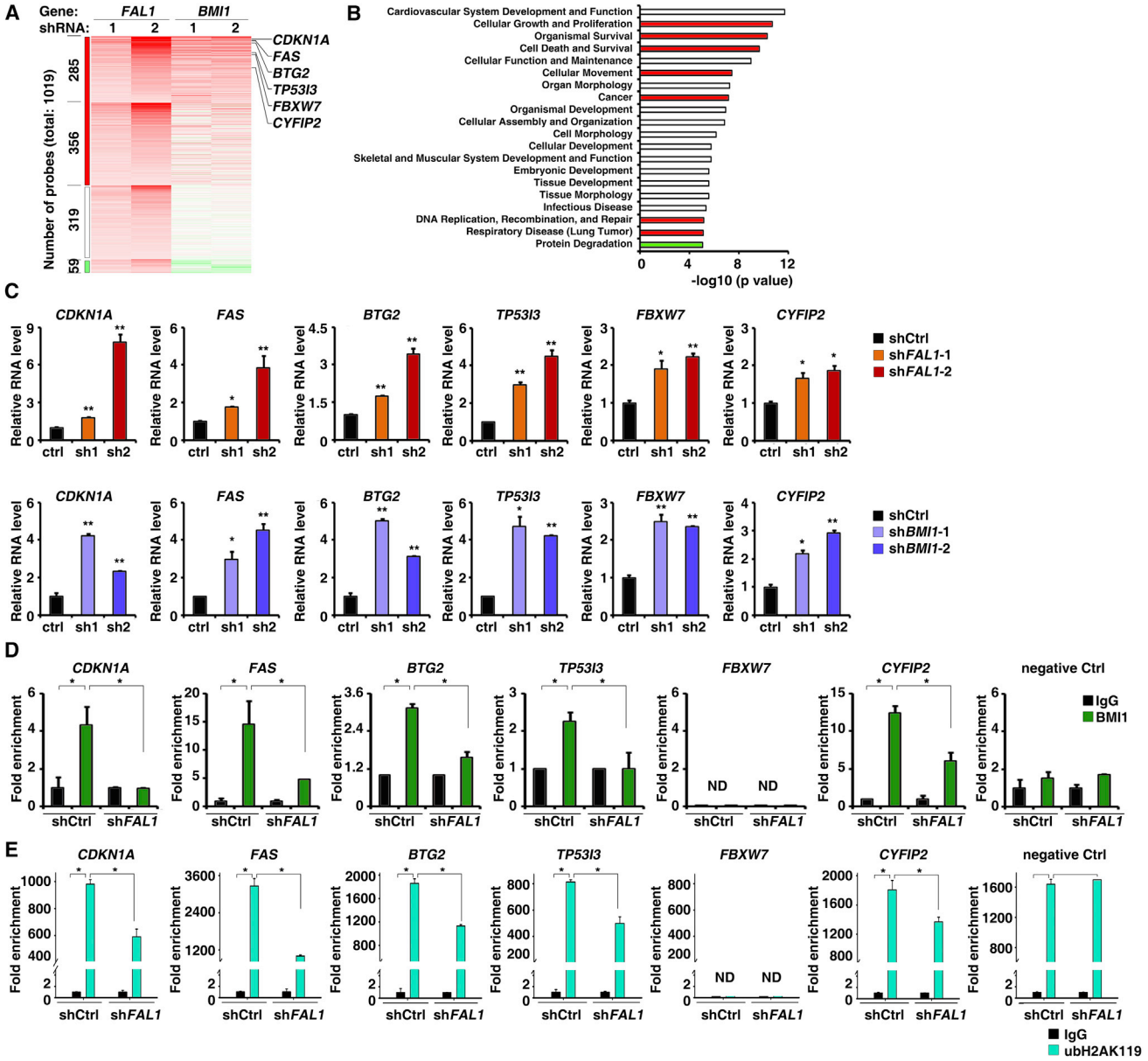

Figure 5. *FAL1* Regulates the Transcription of a Large Number of Genes

(A) Expression heatmap of transcripts whose expressions were upregulated by the transduction of both *FAL1* shRNAs. Expression profiles of the 1,019 probes in cells with *FAL1* knockdown (left) and with BMI1 knockdown (right) are shown. The genes were ranked according to the magnitude of the fold change within the *FAL1* group. Red and green indicate up- and downregulation, respectively.

(B) The top 20 biological processes affected by *FAL1* downregulation by GO.

(C) qRT-PCR validation of six genes that were upregulated by the knockdown of *FAL1* and *BMI1* in the microarray.

(D) The occupancy of BMI1 in the promoter regions of the above six genes was measured by BMI1 ChIP assay followed by qPCR in cells expressing control and *FAL1* shRNA. ND, not detected.

(E) PRC1 complex activity in cells expressing control and *FAL1* shRNAs. The ubiquitination of H2AK119 on the promoters of its target genes were measured by ubH2AK119 ChIP assays followed by qPCR.

Error bars indicate SD. *$p < 0.05$; **$p < 0.01$. See also Table S10.

reduced the occupancy of BMI1 and ubiquitination levels of H2AK119 on the promoter regions of these genes (Figures 5D and 5E). These findings demonstrate that *FAL1* is important in regulating gene transcription, presumably in part by regulating the association between BMI1 and the promoter regions of its target genes.

FAL1 Regulates Cell-Cycle Progression and Senescence via the Suppression of p21 Expression

Among the common targets of *FAL1* and BMI1, *CDKN1A* is of particular interest because of its remarkable expression fold change upon *FAL1* knockdown (Figure 5A) and its significant contribution to tumorigenesis. Furthermore, in ovarian tumor

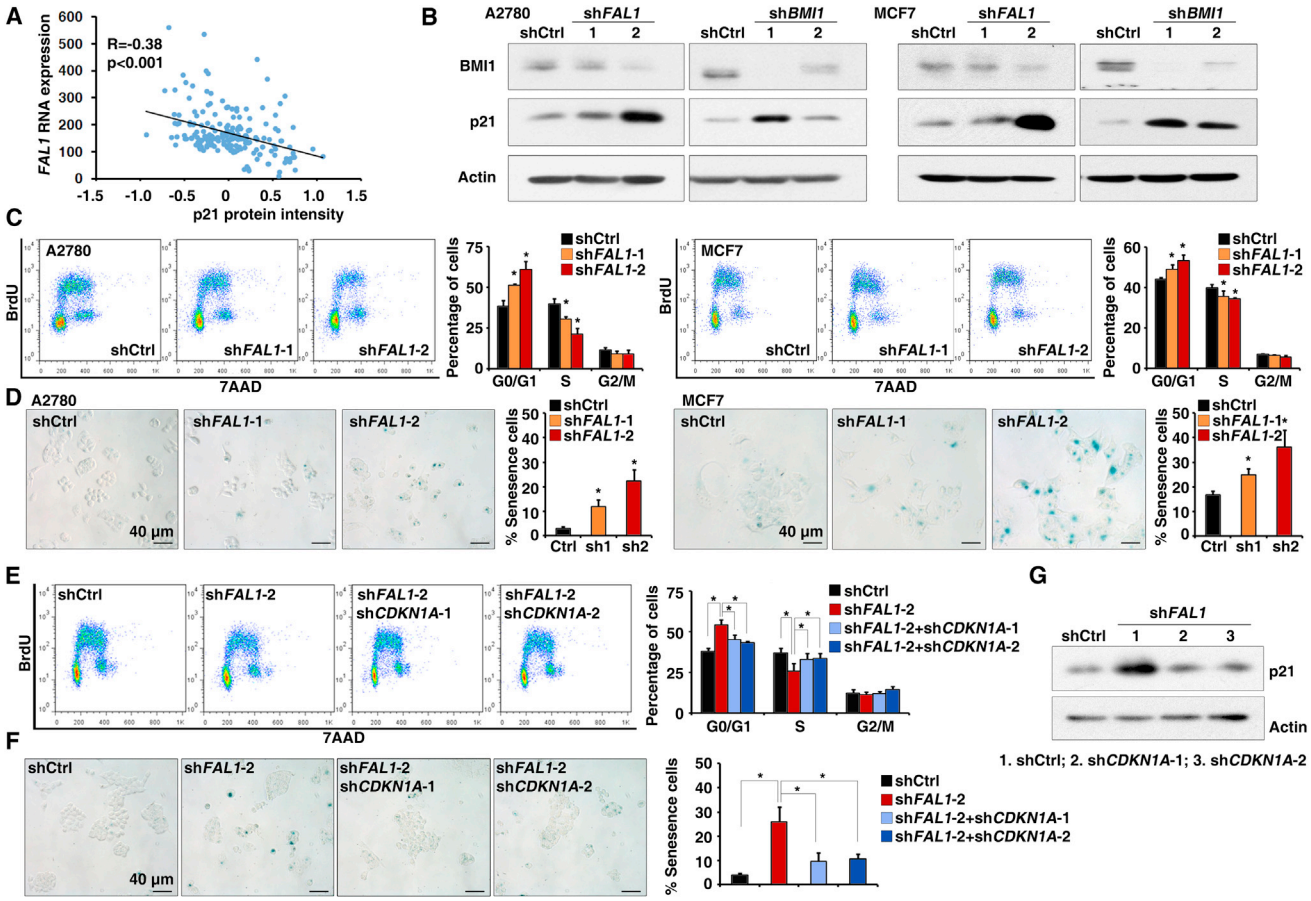

Figure 6. *FAL1* Regulates Cell-Cycle Progression and Senescence via the Suppression of p21 Expression

(A) The correlation between *FAL1* expression and p21 levels in ovarian cancer samples.

(B) Western blot of p21 and BMI1 in cells expressing control, *FAL1* and *BMI1* shRNAs.

(C) Cell-cycle profiles of cells expressing control and *FAL1* shRNAs.

(D) β-Galactosidase staining of cells expressing control and *FAL1* shRNAs.

(E) Cell-cycle profiles of A2780 cells expressing control and *FAL1* shRNAs with and without *CDKN1A* shRNAs.

(F) β-Galactosidase staining of A2780 cells expressing control and *FAL1* shRNAs with and without *CDKN1A* shRNAs.

(G) p21 protein expression of in A2780 control and *FAL1* knockdown cells expressing control and *CDKN1A* shRNAs.

Error bars indicate SD. *p < 0.05. See also Figure S5.

specimens, we detected a significant negative correlation between *FAL1* RNA levels and the expression of p21 in both protein and RNA levels (Figure 6A; Figure S5). It was consistent with our finding that *CDKN1A* mRNA was elevated upon *FAL1* knockdown and strongly suggests that *FAL1* can negatively regulate p21 protein expression in tumors. In support of the role of *FAL1* in the repression of p21 expression, p21 protein was significantly increased in both A2780 and MCF-7 cell lines expressing *FAL1* shRNA (Figure 6B). Because *CDKN1A* is a common target of *FAL1* and BMI1, the expression of p21 was also induced by BMI1 knockdown (Figure 6B). In combination with our earlier results from ChIP assays (Figures 5D and 5E), these findings strongly suggest that *FAL1* may modulate the transcription of *CDKN1A* by regulating BMI1 abundance and occupancy on *CDKN1A*'s promoter.

Next, we examined if knocking down *FAL1* leads to the same two phenotypes often seen in cells with p21 overexpression: cell-cycle arrest and senescence. Using a *BrdU* incorporation assay, we found that knocking down *FAL1* expression by shRNAs significantly induced G0/G1 arrest in both A2780 and MCF7 cell lines (Figure 6C). This is in agreement with our previous observation that *FAL1* knockdown significantly blocked cell proliferation (Figure 2). In addition, we observed that the expression of *FAL1* shRNAs remarkably increased the number of the cells with typical senescence morphology. We also measured the β-galactosidase activity in cancer cells expressing control or *FAL1* shRNAs and found that the percentage of β-galactosidase-positive cancer cells was significantly higher in *FAL1* knockdown cells than in controls (Figure 6D). Finally, we found that knocking down p21 expression significantly rescued the cell cycle and senescence phenotypes that were induced by the expression of *FAL1* shRNAs (Figures 6E–6G). Together, these results demonstrate that *FAL1* exerts its function at least in part via regulating p21 expression.

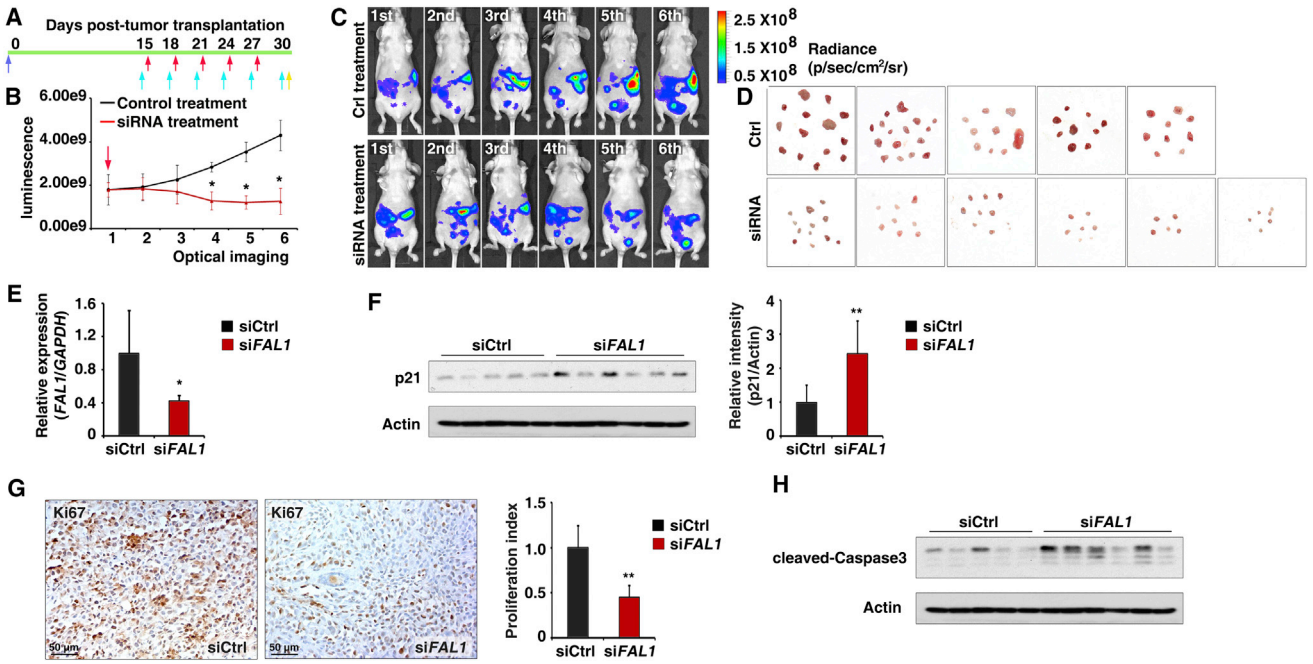

Figure 7. Reduction of *FAL1* Expression by siRNA Delivery Inhibits Orthotopic Ovarian Tumor Growth in Vivo

(A) Illustration of the *FAL1* siRNA treatment timeline. Arrows indicate different events (dark blue, cell injection; light blue, bioluminescent imaging; red, siRNA treatment; yellow, tissue harvesting).

(B) Bioluminescent quantification of tumor growth of *FAL1* and control siRNA-treated mice. The first treatment is indicated by the red arrow. The x axis represents the six rounds of optical imaging measurements.

(C) Representative bioluminescent images of animals receiving control (top) and *FAL1* (bottom) siRNAs during the five rounds of treatments.

(D) Images of tumor nodes collected from animals receiving control (top) and *FAL1* (bottom) siRNA 3 days after the last treatment.

(E and F) The RNA expression of *FAL1* (E) and protein expression of p21 (F) in A2780 tumors.

(G) Cell proliferation in A2780 tumors. (Left) Ki67 staining; (right) quantification of the proliferation rate.

(H) The level of cleaved caspase3 in A2780 tumors.

Error bars indicate SD. *$p < 0.05$; **$p < 0.01$.

Reducing the Expression of *FAL1* by Small Interfering RNA Delivery Inhibits Orthotopic Ovarian Tumor Growth In Vivo

We next evaluated the therapeutic potential of small interfering RNA (siRNA) that specifically targets *FAL1* using an orthotopic mouse model for late-stage ovarian cancer. Briefly, luciferase-expressing A2780 cells were injected into the peritoneal cavity of female nude mice. Two weeks after cell injection, mice were randomly assigned to one of two groups to receiving either *FAL1* siRNA or control siRNA via intraperitoneal injection. Bioluminescent imaging was used to monitor the tumor burden before each round of siRNA injection (Figure 7A). Although there was a significant increase in the intensity of luminescence in the control siRNA-treated animals over the course of the injections, the luminescence signals in the *FAL1* siRNA-treated mice decreased significantly (Figures 7B and 7C). Consistently, the tumor nodes from mice treated with *FAL1* siRNA were much smaller and weighed significantly less than those from the control group (Figure 7D). Consistent with in vitro observation, the p21 expression in *FAL1* siRNA-treated tumors was higher than that in control-treated tumors (Figures 7E and 7F). Furthermore, we found that *FAL1* siRNA-treated tumors had fewer Ki67-positive cells and more apoptosis than controls (Figures 7G and 7H). These results not only confirm the oncogenic activity of *FAL1* in vivo but also suggest that targeting *FAL1* may represent an approach in cancer treatment.

DISCUSSION

Before the discovery of noncoding RNAs, searches for cancer drivers were focused on protein-coding genes that resided in recurrent alterations in cancer genomes. However, many of these recurrent alterations were found to either be in "gene desert" regions or to contain no known cancer-causing protein-coding genes (Beroukhim et al., 2010; Zack et al., 2013). Furthermore, although over 30% of the genome is affected by SCNAs, only 2% of the human genome encodes proteins. These findings, in combination with the recent revelation that about 70% of the human genome is transcribed into RNA, strongly suggest that noncoding RNAs in SCNAs play significant roles in tumor development. However, large-scale functional characterization of lncRNA SCNAs is still lacking (Du et al., 2013). Here, we demonstrated that lncRNA SCNAs are common in cancer genomes; our findings also provide a plausible molecular mechanism underlying the deregulation of cancer-associated lncRNA expression in cancers.

Recent advances in high-throughput biotechnologies have led to the exponential growth of high-resolution SCNA profiles of

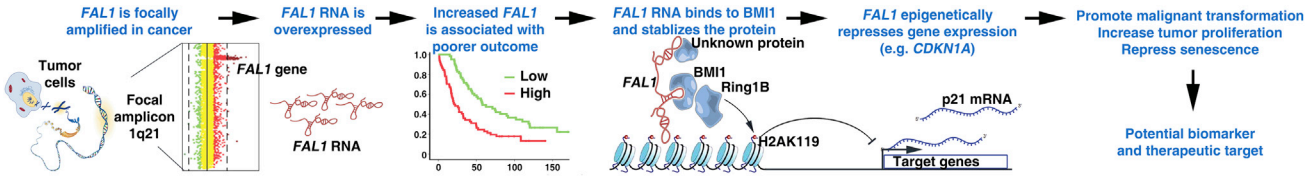

Figure 8. A Proposed Model of the Functional Consequence of *FAL1* Amplification in Tumorigenesis

specimens from various types of cancer. However, because cancer genomes are highly unstable, many cancer-associated alterations are not the causes but instead the consequence of tumorigenesis. The main challenge is to identify the cancer-driving SCNAs, which, once targeted by therapeutic agents, can suppress or eliminate tumor growth. Analyses of genome-wide profiles using various bioinformatics approaches can reveal associations between SCNAs and different types of cancer but cannot distinguish "causal" from "bystander" genetic alterations. Genome-wide functional screening approaches have been used with some success in identifying cancer-driving events; however, this approach can be time and labor intensive and, more important, susceptible to false-positive discovery. Here, we aimed to identify oncogenic lncRNAs using an integrated strategy. The bioinformatics analyses we conducted serve as a powerful clinical filter to eliminate lncRNAs that are less likely to be oncogenes because of the lack of RNA expression or genetic alterations in cancer; consequently, only a subgroup of genes with high oncogenic potential was selected for downstream functional validation. The small size of the candidate gene pool, in return, allowed us to use multiple hairpins for functional validation.

We revealed that *FAL1* can interact with the PRC1 core protein, BMI1, and that *FAL1* exerts its oncogenic function at least in part via suppressing of p21 expression (Figure 8). Previous studies have suggested that a large number of lncRNAs are associated with chromatin-modifying complexes such as PRC2 (Khalil et al., 2009). For example, *HOTAIR* (Tsai et al., 2010) and *ANRIL* (Kotake et al., 2011; Yap et al., 2010), two well-characterized oncogenic lncRNAs, both interact with PRC complexes to regulate gene transcription. Specifically, *HOTAIR*, which is known for its role in promoting tumor metastasis (Gupta et al., 2010), binds to EZH2/PRC2 and LSD1 to coordinate their function in epigenetically regulating gene expression (Tsai et al., 2010), while *ANRIL* interacts with CBX7/PRC1 (Yap et al., 2010) and SUZ12/PRC2 (Kotake et al., 2011) to repress the transcription of the tumor suppressor *INK4A/INK4B*. In addition, the tumor suppressor lncRNA *Xist* can regulate gene expression by tethering PRC2 to the X chromosome (Jeon and Lee, 2011). In combination with these findings, the functional interaction between *FAL1* and BMI1 that we characterized in this study further emphasizes the centrality of lncRNA in the regulation of gene expression and suggests that interaction with chromatic modifying complexes may be an important mechanism by which lncRNAs exert their functions.

Because a large percentage of the human genome encodes noncoding RNAs, and lncRNAs are highly deregulated in cancer, it is believed that lncRNAs represent a class of cancer biomarkers and therapeutic targets whose potential has not been fully explored. Several studies have described specific lncRNAs as cancer biomarkers. The most prominent example is *PCA3*, a lncRNA highly expressed in prostate cancer (Lee et al., 2011). Therapies designed to target cancer-driving lncRNAs are also under intensive investigation. To this end, rapid advances in oligonucleotide and nanoparticle technology create realistic optimism for delivering siRNA-based therapeutics to regulate lncRNA levels in vivo. Our findings warrant further investigation about the potential of *FAL1* as an informative biomarker and a therapeutic target for patients with cancer.

EXPERIMENTAL PROCEDURES

Patient Specimens

Ovarian cancer specimens were collected at the University of Turin. Specimens were acquired and processed under procedures approved by the University of Pennsylvania and University of Turin institutional review boards.

SNP Data Retrieval and Analysis

The raw data from SNP microarrays were downloaded from the Tumorscape database created by the Broad Institute. CEL files were extracted using the Affymetrix Genotype software and analyzed using the Partek Genomics Suite software package. The 158 independent focal genomic alteration peaks and the numbers of protein-coding genes in each peak were previously identified by the Tumorscape Project based on 3,131 cancer specimens of 26 histological types (Beroukhim et al., 2010). Please see Supplemental Experimental Procedures for a discussion of detailed procedures.

shRNA Screening and Lentiviral Transduction

Lentiviral vector (pLKO.1) and packaging vectors were transfected into 293T cells. The medium was changed 8 hr after transfection, and the medium containing lentivirus was collected 48 hr later. Cancer cells were infected with lentivirus in the presence of 8 μg/ml polybrene.

RNA Isolation and qRT-PCR

Total RNA was extracted using TRIzol Reagent (Invitrogen) and reverse transcribed using the High Capacity RNA-to-cDNA Kit (Applied Biosystems). cDNA was quantified by an ABI ViiA 7 System (Applied Biosystems).

RNA Pull-Down Assay

The *FAL1* cDNA was cloned into pBluescript II vector. Biotin-labeled RNAs were transcribed in vitro and purified. Cell nuclei were harvested and resuspended in freshly prepared polysome lysis buffer. Biotinylated RNA (10 pmol) was mixed with 200 μg of nuclear lysate and then mixed with prewashed streptavidin-agarose beads for 1 hr. The beads were washed with ice-cold NT2 buffer five times and then boiled with 2x Laemmli loading buffer.

Xenograft Model In Vivo

Six- to eight-week-old female nude mice were used for the xenograft experiments. Cancer cells were trypsinized and harvested in PBS, and a total volume of 0.1 ml PBS was injected subcutaneously into the flanks or intraperitoneally into the peritoneal cavity. The jetPEI reagent (Polyplus Transfection) was used to deliver the siRNAs in vivo. The animal study protocol was reviewed and

approved by the Institutional Animal Care and Use Committee of the University of Pennsylvania.

Statistical Analysis

Results are expressed as mean ± SD, and $p < 0.05$ indicates significance. The survival curves were constructed according to the Kaplan-Meier method and compared with the log-rank test.

ACCESSION NUMBER

The microarray data are accessible in the Gene Expression Omnibus database under accession number GSE52210.

SUPPLEMENTAL INFORMATION

Supplemental Information includes Supplemental Experimental Procedures, five figures, and ten tables and can be found with this article online at http://dx.doi.org/10.1016/j.ccr.2014.07.009.

ACKNOWLEDGMENTS

We thank the Tumorscape team and Dr. Nelly Auersperg for providing SNP arrays and HOSE cells, respectively. This work was supported, in whole or in part, by the Basser Research Center for BRCA (K.L.N. and L.Z.), the NIH (grant R01CA142776 to L.Z., grant P50CA083638 to J.B. and L.Z., grant P50CA083639 to G.B.M., grant P50CA098258 to G.B.M., grant U24CA143883 to G.B.M., grant P01CA099031 to G.B.M., grant R01CA127334 to H.L., grant R01CA148759 to Q.H., and grant K12HD000849 to J.L.T.), the Ovarian Cancer Research Fund (L.Z. and X.H.), the Breast Cancer Alliance (L.Z.), Department of Defense (L.Z.), and the Marsha Rivkin Center for Ovarian Cancer Research (L.Z.). D.Z. and L.Y were supported by the China Scholarship Council. Functional Proteomics RPPA Core at the MD Anderson Cancer Center provided reverse-phase protein array analysis. The core facility is supported by NIH Cancer Center Support Grant CA016672 through the MD Anderson Cancer Center.

Received: November 14, 2013
Revised: May 17, 2014
Accepted: July 15, 2014
Published: September 8, 2014

REFERENCES

Batista, P.J., and Chang, H.Y. (2013). Long noncoding RNAs: cellular address codes in development and disease. Cell *152*, 1298–1307.

Beroukhim, R., Mermel, C.H., Porter, D., Wei, G., Raychaudhuri, S., Donovan, J., Barretina, J., Boehm, J.S., Dobson, J., Urashima, M., et al. (2010). The landscape of somatic copy-number alteration across human cancers. Nature *463*, 899–905.

Cabili, M.N., Trapnell, C., Goff, L., Koziol, M., Tazon-Vega, B., Regev, A., and Rinn, J.L. (2011). Integrative annotation of human large intergenic noncoding RNAs reveals global properties and specific subclasses. Genes Dev. *25*, 1915–1927.

Carpenter, S., Aiello, D., Atianand, M.K., Ricci, E.P., Gandhi, P., Hall, L.L., Byron, M., Monks, B., Henry-Bezy, M., Lawrence, J.B., et al. (2013). A long noncoding RNA mediates both activation and repression of immune response genes. Science *341*, 789–792.

Derrien, T., Johnson, R., Bussotti, G., Tanzer, A., Djebali, S., Tilgner, H., Guernec, G., Martin, D., Merkel, A., Knowles, D.G., et al. (2012). The GENCODE v7 catalog of human long noncoding RNAs: analysis of their gene structure, evolution, and expression. Genome Res. *22*, 1775–1789.

Di Ruscio, A., Ebralidze, A.K., Benoukraf, T., Amabile, G., Goff, L.A., Terragni, J., Figueroa, M.E., De Figueiredo Pontes, L.L., Alberich-Jorda, M., Zhang, P., et al. (2013). DNMT1-interacting RNAs block gene-specific DNA methylation. Nature *503*, 371–376.

Djebali, S., Davis, C.A., Merkel, A., Dobin, A., Lassmann, T., Mortazavi, A., Tanzer, A., Lagarde, J., Lin, W., Schlesinger, F., et al. (2012). Landscape of transcription in human cells. Nature *489*, 101–108.

Du, Z., Fei, T., Verhaak, R.G., Su, Z., Zhang, Y., Brown, M., Chen, Y., and Liu, X.S. (2013). Integrative genomic analyses reveal clinically relevant long noncoding RNAs in human cancer. Nat. Struct. Mol. Biol. *20*, 908–913.

Engreitz, J.M., Pandya-Jones, A., McDonel, P., Shishkin, A., Sirokman, K., Surka, C., Kadri, S., Xing, J., Goren, A., Lander, E.S., et al. (2013). The Xist lncRNA exploits three-dimensional genome architecture to spread across the X chromosome. Science *341*, 1237973.

Gomez, J.A., Wapinski, O.L., Yang, Y.W., Bureau, J.F., Gopinath, S., Monack, D.M., Chang, H.Y., Brahic, M., and Kirkegaard, K. (2013). The NeST long ncRNA controls microbial susceptibility and epigenetic activation of the interferon-γ locus. Cell *152*, 743–754.

Gupta, R.A., Shah, N., Wang, K.C., Kim, J., Horlings, H.M., Wong, D.J., Tsai, M.C., Hung, T., Argani, P., Rinn, J.L., et al. (2010). Long non-coding RNA HOTAIR reprograms chromatin state to promote cancer metastasis. Nature *464*, 1071–1076.

Guttman, M., and Rinn, J.L. (2012). Modular regulatory principles of large non-coding RNAs. Nature *482*, 339–346.

Guttman, M., Amit, I., Garber, M., French, C., Lin, M.F., Feldser, D., Huarte, M., Zuk, O., Carey, B.W., Cassady, J.P., et al. (2009). Chromatin signature reveals over a thousand highly conserved large non-coding RNAs in mammals. Nature *458*, 223–227.

Guttman, M., Donaghey, J., Carey, B.W., Garber, M., Grenier, J.K., Munson, G., Young, G., Lucas, A.B., Ach, R., Bruhn, L., et al. (2011). lincRNAs act in the circuitry controlling pluripotency and differentiation. Nature *477*, 295–300.

Hansen, T.B., Jensen, T.I., Clausen, B.H., Bramsen, J.B., Finsen, B., Damgaard, C.K., and Kjems, J. (2013). Natural RNA circles function as efficient microRNA sponges. Nature *495*, 384–388.

Huarte, M., Guttman, M., Feldser, D., Garber, M., Koziol, M.J., Kenzelmann-Broz, D., Khalil, A.M., Zuk, O., Amit, I., Rabani, M., et al. (2010). A large intergenic noncoding RNA induced by p53 mediates global gene repression in the p53 response. Cell *142*, 409–419.

Hung, T., Wang, Y., Lin, M.F., Koegel, A.K., Kotake, Y., Grant, G.D., Horlings, H.M., Shah, N., Umbricht, C., Wang, P., et al. (2011). Extensive and coordinated transcription of noncoding RNAs within cell-cycle promoters. Nat. Genet. *43*, 621–629.

International Human Genome Sequencing Consortium (2004). Finishing the euchromatic sequence of the human genome. Nature *431*, 931–945.

Jeon, Y., and Lee, J.T. (2011). YY1 tethers Xist RNA to the inactive X nucleation center. Cell *146*, 119–133.

Ji, P., Diederichs, S., Wang, W., Böing, S., Metzger, R., Schneider, P.M., Tidow, N., Brandt, B., Buerger, H., Bulk, E., et al. (2003). MALAT-1, a novel noncoding RNA, and thymosin beta4 predict metastasis and survival in early-stage non-small cell lung cancer. Oncogene *22*, 8031–8041.

Karreth, F.A., and Pandolfi, P.P. (2013). ceRNA cross-talk in cancer: when ce-bling rivalries go awry. Cancer Discov. *3*, 1113–1121.

Khalil, A.M., Guttman, M., Huarte, M., Garber, M., Raj, A., Rivea Morales, D., Thomas, K., Presser, A., Bernstein, B.E., van Oudenaarden, A., et al. (2009). Many human large intergenic noncoding RNAs associate with chromatin-modifying complexes and affect gene expression. Proc. Natl. Acad. Sci. USA *106*, 11667–11672.

Kim, T.K., Hemberg, M., Gray, J.M., Costa, A.M., Bear, D.M., Wu, J., Harmin, D.A., Laptewicz, M., Barbara-Haley, K., Kuersten, S., et al. (2010). Widespread transcription at neuronal activity-regulated enhancers. Nature *465*, 182–187.

Kim, T., Cui, R., Jeon, Y.J., Lee, J.H., Lee, J.H., Sim, H., Park, J.K., Fadda, P., Tili, E., Nakanishi, H., et al. (2014). Long-range interaction and correlation between MYC enhancer and oncogenic long noncoding RNA CARLo-5. Proc. Natl. Acad. Sci. USA *111*, 4173–4178.

Kotake, Y., Nakagawa, T., Kitagawa, K., Suzuki, S., Liu, N., Kitagawa, M., and Xiong, Y. (2011). Long non-coding RNA ANRIL is required for the PRC2 recruitment to and silencing of p15(INK4B) tumor suppressor gene. Oncogene *30*, 1956–1962.

Kretz, M., Siprashvili, Z., Chu, C., Webster, D.E., Zehnder, A., Qu, K., Lee, C.S., Flockhart, R.J., Groff, A.F., Chow, J., et al. (2013). Control of somatic tissue differentiation by the long non-coding RNA TINCR. Nature *493*, 231–235.

Lai, F., Orom, U.A., Cesaroni, M., Beringer, M., Taatjes, D.J., Blobel, G.A., and Shiekhattar, R. (2013). Activating RNAs associate with Mediator to enhance chromatin architecture and transcription. Nature *494*, 497–501.

Lee, J.T. (2012). Epigenetic regulation by long noncoding RNAs. Science *338*, 1435–1439.

Lee, G.L., Dobi, A., and Srivastava, S. (2011). Prostate cancer: diagnostic performance of the PCA3 urine test. Nat. Rev. Urol. *8*, 123–124.

Li, W., Notani, D., Ma, Q., Tanasa, B., Nunez, E., Chen, A.Y., Merkurjev, D., Zhang, J., Ohgi, K., Song, X., et al. (2013). Functional roles of enhancer RNAs for oestrogen-dependent transcriptional activation. Nature *498*, 516–520.

Lieberman, J., Slack, F., Pandolfi, P.P., Chinnaiyan, A., Agami, R., and Mendell, J.T. (2013). Noncoding RNAs and cancer. Cell *153*, 9–10.

Ling, H., Spizzo, R., Atlasi, Y., Nicoloso, M., Shimizu, M., Redis, R.S., Nishida, N., Gafà, R., Song, J., Guo, Z., et al. (2013). CCAT2, a novel noncoding RNA mapping to 8q24, underlies metastatic progression and chromosomal instability in colon cancer. Genome Res. *23*, 1446–1461.

Loewer, S., Cabili, M.N., Guttman, M., Loh, Y.H., Thomas, K., Park, I.H., Garber, M., Curran, M., Onder, T., Agarwal, S., et al. (2010). Large intergenic non-coding RNA-RoR modulates reprogramming of human induced pluripotent stem cells. Nat. Genet. *42*, 1113–1117.

Memczak, S., Jens, M., Elefsinioti, A., Torti, F., Krueger, J., Rybak, A., Maier, L., Mackowiak, S.D., Gregersen, L.H., Munschauer, M., et al. (2013). Circular RNAs are a large class of animal RNAs with regulatory potency. Nature *495*, 333–338.

Ørom, U.A., and Shiekhattar, R. (2013). Long noncoding RNAs usher in a new era in the biology of enhancers. Cell *154*, 1190–1193.

Ørom, U.A., Derrien, T., Beringer, M., Gumireddy, K., Gardini, A., Bussotti, G., Lai, F., Zytnicki, M., Notredame, C., Huang, Q., et al. (2010). Long noncoding RNAs with enhancer-like function in human cells. Cell *143*, 46–58.

Pasmant, E., Laurendeau, I., Héron, D., Vidaud, M., Vidaud, D., and Bièche, I. (2007). Characterization of a germ-line deletion, including the entire INK4/ARF locus, in a melanoma-neural system tumor family: identification of ANRIL, an antisense noncoding RNA whose expression coclusters with ARF. Cancer Res. *67*, 3963–3969.

Poliseno, L., Salmena, L., Zhang, J., Carver, B., Haveman, W.J., and Pandolfi, P.P. (2010). A coding-independent function of gene and pseudogene mRNAs regulates tumour biology. Nature *465*, 1033–1038.

Prensner, J.R., and Chinnaiyan, A.M. (2011). The emergence of lncRNAs in cancer biology. Cancer Discov. *1*, 391–407.

Prensner, J.R., Iyer, M.K., Balbin, O.A., Dhanasekaran, S.M., Cao, Q., Brenner, J.C., Laxman, B., Asangani, I.A., Grasso, C.S., Kominsky, H.D., et al. (2011). Transcriptome sequencing across a prostate cancer cohort identifies PCAT-1, an unannotated lincRNA implicated in disease progression. Nat. Biotechnol. *29*, 742–749.

Prensner, J.R., Iyer, M.K., Sahu, A., Asangani, I.A., Cao, Q., Patel, L., Vergara, I.A., Davicioni, E., Erho, N., Ghadessi, M., et al. (2013). The long noncoding RNA SChLAP1 promotes aggressive prostate cancer and antagonizes the SWI/SNF complex. Nat. Genet. *45*, 1392–1398.

Schuettengruber, B., Chourrout, D., Vervoort, M., Leblanc, B., and Cavalli, G. (2007). Genome regulation by polycomb and trithorax proteins. Cell *128*, 735–745.

Simon, M.D., Pinter, S.F., Fang, R., Sarma, K., Rutenberg-Schoenberg, M., Bowman, S.K., Kesner, B.A., Maier, V.K., Kingston, R.E., and Lee, J.T. (2013). High-resolution Xist binding maps reveal two-step spreading during X-chromosome inactivation. Nature *504*, 465–469.

Tay, Y., Kats, L., Salmena, L., Weiss, D., Tan, S.M., Ala, U., Karreth, F., Poliseno, L., Provero, P., Di Cunto, F., et al. (2011). Coding-independent regulation of the tumor suppressor PTEN by competing endogenous mRNAs. Cell *147*, 344–357.

Tripathi, V., Ellis, J.D., Shen, Z., Song, D.Y., Pan, Q., Watt, A.T., Freier, S.M., Bennett, C.F., Sharma, A., Bubulya, P.A., et al. (2010). The nuclear-retained noncoding RNA MALAT1 regulates alternative splicing by modulating SR splicing factor phosphorylation. Mol. Cell *39*, 925–938.

Tripathi, V., Shen, Z., Chakraborty, A., Giri, S., Freier, S.M., Wu, X., Zhang, Y., Gorospe, M., Prasanth, S.G., Lal, A., and Prasanth, K.V. (2013). Long noncoding RNA MALAT1 controls cell cycle progression by regulating the expression of oncogenic transcription factor B-MYB. PLoS Genet. *9*, e1003368.

Tsai, M.C., Manor, O., Wan, Y., Mosammaparast, N., Wang, J.K., Lan, F., Shi, Y., Segal, E., and Chang, H.Y. (2010). Long noncoding RNA as modular scaffold of histone modification complexes. Science *329*, 689–693.

Ulitsky, I., and Bartel, D.P. (2013). lincRNAs: genomics, evolution, and mechanisms. Cell *154*, 26–46.

Ulitsky, I., Shkumatava, A., Jan, C.H., Sive, H., and Bartel, D.P. (2011). Conserved function of lincRNAs in vertebrate embryonic development despite rapid sequence evolution. Cell *147*, 1537–1550.

Wang, D., Garcia-Bassets, I., Benner, C., Li, W., Su, X., Zhou, Y., Qiu, J., Liu, W., Kaikkonen, M.U., Ohgi, K.A., et al. (2011). Reprogramming transcription by distinct classes of enhancers functionally defined by eRNA. Nature *474*, 390–394.

Yang, L., Lin, C., Liu, W., Zhang, J., Ohgi, K.A., Grinstein, J.D., Dorrestein, P.C., and Rosenfeld, M.G. (2011). ncRNA- and Pc2 methylation-dependent gene relocation between nuclear structures mediates gene activation programs. Cell *147*, 773–788.

Yang, F., Huo, X.S., Yuan, S.X., Zhang, L., Zhou, W.P., Wang, F., and Sun, S.H. (2013a). Repression of the long noncoding RNA-LET by histone deacetylase 3 contributes to hypoxia-mediated metastasis. Mol. Cell *49*, 1083–1096.

Yang, L., Lin, C., Jin, C., Yang, J.C., Tanasa, B., Li, W., Merkurjev, D., Ohgi, K.A., Meng, D., Zhang, J., et al. (2013b). lncRNA-dependent mechanisms of androgen-receptor-regulated gene activation programs. Nature *500*, 598–602.

Yap, K.L., Li, S., Muñoz-Cabello, A.M., Raguz, S., Zeng, L., Mujtaba, S., Gil, J., Walsh, M.J., and Zhou, M.M. (2010). Molecular interplay of the noncoding RNA ANRIL and methylated histone H3 lysine 27 by polycomb CBX7 in transcriptional silencing of INK4a. Mol. Cell *38*, 662–674.

Yildirim, E., Kirby, J.E., Brown, D.E., Mercier, F.E., Sadreyev, R.I., Scadden, D.T., and Lee, J.T. (2013). Xist RNA is a potent suppressor of hematologic cancer in mice. Cell *152*, 727–742.

Zack, T.I., Schumacher, S.E., Carter, S.L., Cherniack, A.D., Saksena, G., Tabak, B., Lawrence, M.S., Zhang, C.Z., Wala, J., Mermel, C.H., et al. (2013). Pan-cancer patterns of somatic copy number alteration. Nat. Genet. *45*, 1134–1140.